Space Sci Rev (2018) 214:100
https://doi.org/10.1007/s11214-018-0530-5

The Rotation and Interior Structure Experiment on the InSight Mission to Mars

William M. Folkner[1] · **Véronique Dehant**[2] · **Sébastien Le Maistre**[2] · **Marie Yseboodt**[2] · **Attilio Rivoldini**[2] · **Tim Van Hoolst**[2] · **Sami W. Asmar**[1] · **Matthew P. Golombek**[1]

Received: 2 March 2018 / Accepted: 25 July 2018

Abstract The Rotation and Interior Structure Experiment (RISE) on-board the InSight mission will use the lander's X-band (8 GHz) radio system in combination with tracking stations of the NASA Deep Space Network (DSN) to determine the rotation of Mars. RISE will measure the nutation of the Martian spin axis, detecting for the first time the effect of the liquid core of Mars and providing in turn new constraints on the core radius and density. RISE will also measure changes in the rotation rate of Mars on seasonal time-scales thereby constraining the atmospheric angular momentum budget. Finally, RISE will provide a superb tie between the cartographic and inertial reference frames. This paper describes the RISE scientific objectives and measurements, and provides the expected results of the experiment.

Keywords InSight · Mars · Physical properties · Interior structure · Radio science

1 Introduction

The InSight mission will arrive at Mars in November 2018 (Banerdt et al. 2018, this issue). The payload is focused on probing the deep interior of Mars. It consists of a seismometer, a heat flow probe and a radio transponder that allows precise tracking of Mars' rotation. In addition, it has a set of instruments to monitor the local environment (atmospheric pressure, wind, air and ground temperature, magnetic field, cameras), which measure meteorological and magnetic noise sources for the other instruments. Science observations are planned for one Martian year.

The gravitational torque exerted by the Sun on the equatorial bulge of the rotating Mars causes a precession of the axis of rotation in space. The spin axis completes one rotation

The InSight Mission to Mars II
Edited by William B. Banerdt and Christopher T. Russell

✉ W.M. Folkner
william.m.folkner@jpl.nasa.gov

1 Jet Propulsion Laboratory, California Institute of Technology, Pasadena, CA 91109, USA

2 Royal Observatory of Belgium, av. Circulaire 3, Brussels 1180, Belgium

Published online: 09 August 2018

about the normal to the orbit plane in about 171,000 years. Variations in the torque due to the relative positions between Mars and the Sun lead to additional periodic time variations of the rotation axis, the nutations, of which the periods are mainly annual, semi-annual, ter-annual (three times per year) and quarter-annual. The precession rate is a key indicator of Mars' global moment of inertia, whereas nutations are key indicators of the core moment of inertia and the state of the core. A fluid core results in larger nutation amplitudes due to the existence of a resonance effect that only exists if the core is at least partially liquid and that depends on the core's moments of inertia and elastic properties (Le Maistre et al. 2012).

The Rotation and Interior Structure Experiment (RISE) primarily aims at determining the effect of the liquid core on the nutation in order to infer knowledge about the interior structure of Mars. The Martian precession rate has been precisely estimated earlier from Doppler data taken from the Viking and Mars Pathfinder landers (Yoder and Standish 1997; Folkner et al. 1997), from the Mars Exploration Rovers (Kuchynka et al. 2014), and from the Mars Global Surveyor, Mars Odyssey, and Mars Reconnaissance Orbiter spacecraft (Konopliv et al. 2006, 2011, 2016). Unlike the precession rate, the nutation amplitudes have never been measured.

Today, the most meaningful inferences about the core are obtained from the tidal Love number k_2 and to a lesser extent from the moment of inertia of the planet (e.g. Rivoldini et al. 2011). The direct effect of tides is small and has not yet been detected (Van Hoolst et al. 2003), but tides also induce a secular drift in the inclination of the spacecraft orbit (Yoder et al. 2003). This long-period weak signature has been determined from orbiter tracking data and requires careful modeling and precise knowledge about other effects that produce a similar signature (Yoder et al. 2003). Even though the most recent estimates of k_2 agree with each other (Konopliv et al. 2016; Genova et al. 2016), the determination remains challenging. Precisely measuring the nutation of Mars will provide an independent estimation of the core radius and will also constrain the moment of inertia of the core. The precision is expected to be high enough to determine the core radius more precisely than from tides (e.g. Fig. 8 from Rivoldini et al. 2011).

The RISE measurements are the two-way Doppler shifts measured at the Deep Space Network (DSN) stations of a radio signal sent by the DSN to the InSight lander and coherently re-transmitted back to the DSN. The DSN station measures the phase of the spacecraft signal relative to the transmitted signal, and forms a measurement based on the difference in phase shift divided by the integration time (typically 60 seconds). Measurements will be made during several hour-long tracking passes per week during the Instrument Deployment Phase and daily hour-long tracking passes during the subsequent Science Monitoring Phase. The tracking pass duration is limited primarily by the energy available on the lander. The Doppler measurements over the Martian year are sensitive to the changes in direction of the Martian spin axis due to precession and nutation as well as changes in the length-of-day.

The estimated precession and nutation will be interpreted in terms of core properties by making use of constraints deduced about Mars' silicate shell from the InSight seismometer experiment SEIS (Lognonne et al. 2018) and heat flow probe HP^3 (see Plesa et al. 2016; Morgan et al. 2017; Spohn et al. 2018). The length-of-day variations are driven primarily by seasonal redistribution of CO_2 between the atmosphere and the ice caps. These seasonal changes have been detected previously and compared with predictions based on General Circulation Models (GCM) of the Martian atmosphere (e.g. Chao and Rubincam 1990; Yoder and Standish 1997; Cazenave and Balmino 1981; Defraigne et al. 2000; Konopliv et al. 2011; Barriot et al. 2001; Van den Acker et al. 2002; Karatekin et al. 2006, 2011). InSight will be more sensitive to these effects than previous missions. InSight will provide an improved global assessment of the CO_2 exchange between the atmosphere and icecaps. This will further be addressed in another paper (Spiga et al. 2018).

2 Nutation and Interior Structure

Nutation provides insight into the interior of Mars through the amplification of the nutation amplitudes that are near resonance with the Free Core Nutation (FCN), one of the rotational normal modes of Mars (e.g. Dehant and Mathews 2015). The frequency of the FCN depends on the interior structure of the planet and in particular on the polar moment of inertia of the core C_f, its equatorial moment of inertia A_f, its dynamical flattening $e_f = (C_f - A_f)/A_f$ and the capacity of its interface with the mantle to deform due to rotation rate variation of the core characterized by the compliance β, with expected value between 0.00015 and 0.00045 (Dehant and Mathews 2015, Chap. 6). Correct up to the first order in the flattening (e.g. Van Hoolst and Dehant 2002), the frequency of the FCN can be written with respect to an inertial frame as

$$\omega_{FCN} = -\Omega \frac{A_f}{A - A_f}(e_f - \beta) \tag{1}$$

where Ω is the mean rotation rate of the planet and A the equatorial moment of inertia. The prograde and retrograde nutation amplitude P' and R' as a function of the nutation frequency ω are usually written as (e.g. Mathews et al. 1991a)

$$P'(\omega) = T_F(\omega)P(\omega) \quad \text{and} \quad R'(\omega) = T_F(-\omega)R(\omega) \tag{2}$$

where P and R represent the prograde and retrograde nutation amplitudes of a rigid planet with the same mass, radius, and flattening as Mars and T_F is a transfer function depending on the interior structure of the planet. The amplitudes and periods of the principal rigid nutations are given in Table 1. The prograde and retrograde amplitude are taken from Roosbeek (1999) and are rescaled using the latest polar moment of inertia (MOI) (Konopliv et al. 2016). The transformation from prograde/retrograde nutations to nutations in obliquity and longitude can be found for example in Dehant and Mathews (2015). The rigid nutation series amplitudes are predicted with an accuracy of 0.1 milliarcseconds (0.1 mas) (Roosbeek 1999) that is one order of magnitude smaller than the accuracy with which RISE will determine the rotation parameters of Mars.

The presence of an inner core would induce a supplemental rotation normal mode called the Free Inner Core Nutation (FICN) (e.g. Mathews et al. 1991a). The FICN rotational mode can have a period close to the period of the annual prograde nutation and could induce a resonant amplification of that nutation large enough to be detectable by RISE (Defraigne et al. 2003). However, the short and very early episode of a core-generated magnetic field and its present-day absence argue against the presence of an inner core. Additionally, constraints about the core radius and composition (close to the eutectic composition of Fe-S) deduced from recent geodesy data (Rivoldini et al. 2011; Khan et al. 2018) would require low core temperatures. Recent thermal evolution studies of Mars (Plesa et al. 2016) indicate that interior temperatures are too high for inner core formation.

Table 1 Periods (in days) and amplitudes (in milliarcseconds, mas) of principal rigid prograde (P) and retrograde (R) nutations

	Period (days)	Prograde (mas)	Retrograde (mas)
1	686.98	103	137
2	343.49	500	18
3	228.99	108	5
4	171.74	18	1

The solutions of the Liouville equations for an elastic two-layer planet with a deformable mantle and a liquid core provide expressions for the wobble; these expressions can be divided by the solutions for a rigid planet in order to get the transfer function (see Sasao et al. 1980, also in Dehant and Mathews 2015):

$$T_F(\omega) = 1 + \frac{\kappa}{e}\frac{\omega}{\Omega} + \frac{A_f}{A - A_f}\left(1 - \frac{\beta}{e} + \frac{\beta - \kappa}{e}\frac{\omega}{\Omega}\right)\frac{\omega}{\omega - \omega_{FCN}} \tag{3}$$

where $e = (C - A)/A$ is the dynamical flattening of the planet and κ and β are compliances characterizing the tidal deformation of the whole planet and the core-mantle boundary respectively. In the frequency band of the principal nutations, ω/Ω is small and thus terms in Eq. (3) that are proportional to ω/Ω can be neglected since they affect the transfer function T_F by less than 0.5%. The simplified transfer function is then:

$$T_F(\omega) = 1 + \frac{A_f}{A - A_f}\left(1 - \frac{\beta}{e}\right)\frac{\omega}{\omega - \omega_{FCN}} = 1 + F\frac{\omega}{\omega - \omega_{FCN}} \tag{4}$$

where F is the liquid-core amplification factor.

To illustrate the dependence of the nutation amplitude on the interior structure of Mars we calculate F and the period of the FCN for a large set of plausible interior structure models of Mars. We employ the same five mantle mineralogies used in Panning et al. (2017) and use a hot and a cold mantle temperature deduced from a recent study about the thermal evolution of Mars (Plesa et al. 2016). The mantle mineralogy models have been calculated with PerpleX (Connolly 2005) using compositions obtained from studies that take into account results from chemical (Dreibus and Wanke 1985; Taylor 2013) and isotopic determinations (Sanloup et al. 1999; Lodders and Fegley 1997; Mohapatra and Murty 2003) of Martian meteorites, in situ samples, and Mars formation scenarios (Morgan and Anders 1979). The mantle compositions include SiO_2 (41.6% to 47.1%), MgO (27.3% to 30.2%), FeO (15.8% to 17.9%), Al_2O_3 (2.5% to 6.4%), CaO (1.9% to 5.2%), and Na_2O (0.1% to 1.2%). We assume that the core of Mars is entirely liquid and convecting and that it contains sulfur as the only light element. To model its properties, we follow Rivoldini and Van Hoolst (2013). The crust in our models is uniform and we allow for densities that are between 2700 kg/m^3 and 3100 kg/m^3 and for a thickness range of 30–90 km (Wieczorek and Zuber 2014). To calculate the dynamic flattening of the models we assume a hydrostatic shape for the planet. The figure of the planet is computed by solving Clairaut's equation to first-order in flattening (e.g. Dahlen and Tromp 1998).

The presence of a partial melt layer in the mantle could significantly modify the rheology of the mantle and the compliances κ and β, but would only weakly affect the core amplification factor F and the FCN frequency since both depend mainly on the dynamic flattening (of the planet and the core) and moments of inertia. The effect of the rheology on core radius inferences from nutations can further be mitigated by modeling the mantle rheology in agreement with the tidal dissipation factor of Mars.

The liquid-core amplification factor F increases with core radius (Figs. 1a and 1b) since the equatorial moment of inertia of the mantle $A - A_f$ decreases with increasing core radius (see Eq. (4)). The FCN period also increases with increasing core radius because the dynamical flattening of the core mantle boundary increases faster than the moment inertia of the mantle (see Eq. (1)). Since the FCN periods of the Mars models lie between the periods of the retrograde semi-annual and ter-annual rigid nutations (−343.5 days, −229 days), those nutations are the most affected by the liquid core. It also follows that with increasing core radius the resonant amplification of the retrograde ter-annual nutations increases and

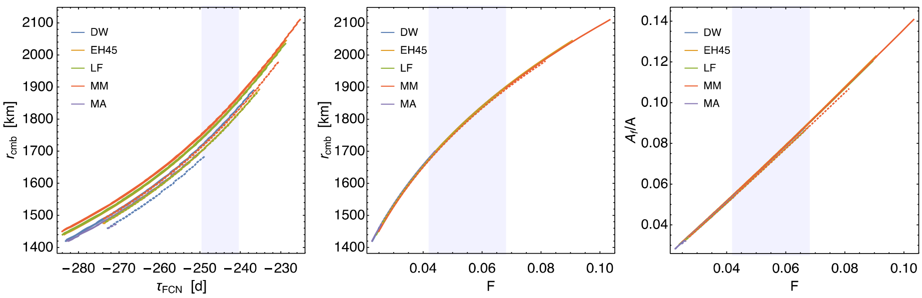

Fig. 1 Left: core radius as a function of FCN period in days; middle: core radius as a function of liquid core amplification factor F; and right: ratio of core and total equatorial moments of inertia A_f/A as a function of F, for the hot (solid curves) and cold (dashed curves) mantle temperature profile. The acronyms stand for the different mantle mineralogy models (DW: Taylor (2013), EH45: Sanloup et al. (1999), LF: Lodders and Fegley (1997), MM: Mohapatra and Murty (2003), MA: Morgan and Anders (1979)). The models agree at 1σ level with the average moment of inertia of Mars (MOI = 0.3637 ± 0.0001) (Konopliv et al. 2016). The uncertainty in expected FCN period and F around a nominal value are indicated by the blue-shaded regions

the retrograde semi-annual nutation decreases. Figure 1b shows that the liquid core amplification factor F is not sensitive to the crust and mantle assumptions. The FCN period is more sensitive to the mineralogy and temperature of the mantle (Fig. 1a) since the dynamical flattening of the core e_f, which depends on the core density, varies strongly with core and mantle composition.

Core radius inferences using the FCN period depend almost linearly on the dynamic flattening of the core and thus are biased by assumptions about the core's dynamic figure (i.e. deviation from hydrostaticity). The deviation of the figure of the core from a hydrostatic shape is unknown. A deviation of about 5%, as has been estimated for the Earth's core (Mathews et al. 1991b), would effectively double the uncertainty on the core radius as inferred from the FCN period estimated by RISE with respect to the results presented in Fig. 1a assuming hydrostatic equilibrium.

The best information on the core radius will be obtained from the core amplification factor F, which does not directly depend on the dynamic flattening of the core and therefore gives a robust core radius estimate. By combining expected results from the seismometer experiment (Lognonne et al. 2018) and measurements of tides (Konopliv et al. 2016) with F and the FCN, the degree of departure from hydrostatic value of the dynamic flattening of the core could also be constrained.

3 Experiment Description

The InSight landing site will be in Elysium Planitia (∼600 km north of the Curiosity rover), with a latitude of 4.5°N and a longitude of 136°E (Golombek et al. 2017). The nominal landing date is November 26, 2018. Science operations will start 46 days later, after the deployment of the instruments.

The InSight lander after deployment is shown in Fig. 2, together with the fields of view of the RISE antennas. The InSight landing system will control its azimuth during landing so the instruments will be deployed to the south. Below the top deck is a thermally-controlled enclosure that includes the Small Deep-Space Transponder (SDST) and a solid-state power amplifier (SSPA) used for the RISE experiment. These are connected to two medium-gain

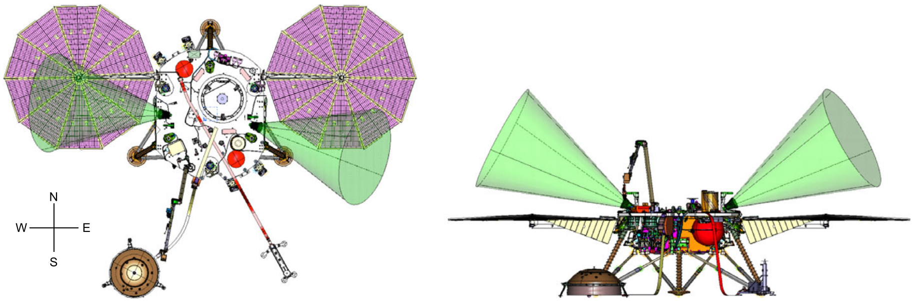

Fig. 2 Left: lander viewed from above with solar panels aligned with the east-west axis and the SEIS and HP^3 instruments deployed to the south (bottom of figure). The beam patterns of the two MGAs are shown, one pointed 15.5° south of due east, the other pointed 6° north of due west. Right: lander viewed from the south showing the elevation of the MGA beam patterns centered 30° in elevation

antennas (MGA) mounted on top of the main deck with fixed pointing directions. The MGA gain pattern provides more than 5 dB of gain for angles 25° off bore sight, that allows for tilts at landing site up to 15° (Golombek et al. 2017). Both antennas have the central gain axis 30° in elevation above the deck. One antenna points 15.5° south of due east and the other point 6° north of due west. These angles were designed to provide good viewing geometry for RISE while also allowing low-rate telemetry from Earth to the lander throughout the mission. Usually the lander is commanded, as needed using the signal transmitted from the DSN. Data from the lander will normally be transmitted to a Mars orbiter using a separate UHF radio system with the orbiter in turn sending the data to Earth.

The SDST receives an X-band carrier signal from a DSN tracking station near 7.2 GHz and transmits a signal back to the tracking station at 8.4 GHz after amplification by the SSPA. The signal transmitted by the SDST is coherent in phase with the signal received from Earth and multiplied by the ratio of 880/749. The station measures the Doppler shift of the round-trip signal, which is proportional to the lander velocity along the line of sight. This radio configuration is similar to that used for Mars Pathfinder and the Mars Exploration Rovers except that InSight uses two fixed medium-gain antennas rather than the steerable high-gain antennas used for those earlier missions.

The Doppler measurement accuracy for RISE will be primarily limited by fluctuations in the number of electrons between Earth and Mars (solar plasma) affecting the speed of radio propagation, and by fluctuations on water vapor content in the Earth troposphere. The noise due to solar plasma depends on the position of Earth and Mars relative to the Sun, often characterized by the Sun-Earth-Probe (SEP) angle while the noise due to water vapor fluctuations are generally larger during the daytime when the atmosphere is warmer and supports higher water vapor content (Asmar et al. 2005). The Earth's dry troposphere and average wet troposphere contribute a significant signature in the Doppler data but can be calibrated to below the expected noise level using signals from the GPS satellite constellation recorded each day at the tracking station (Bar-Sever et al. 2007). Similarly the Earth ionosphere causes a signature in the Doppler data approximately ten times smaller than the troposphere signature and is calibrated with GPS data (Mannucci et al. 1998). The noise due to fluctuations in the dry troposphere and ionosphere are below the noise from the fluctuations in the water vapor density. The Martian troposphere with surface pressure about 6 mbar causes a signature in the Doppler that is near the Doppler noise level and can be calibrated using surface pressure and temperature measurements by InSight. The noise due to fluctuations in the Martian troposphere is well below the noise due to Earth water vapor fluctuations. The Martian ionosphere causes a signature in the Doppler data approximately five times lower than the signature from the Martian troposphere (Lillis et al. 2010). This is near the limit of the Doppler noise and may need to be calibrated with a model (Chapman 1931; Bergeot et al. 2016). Other noise sources are also below the fluctuations from water vapor including fluctuations in the DSN clock frequency, thermal noise in the measurements of radio signal carrier phase at the DSN station and in the SDST due to the finite signal-to-noise ratio and noise in the phase-locked loop in the transponder.

The measured Doppler shift is proportional to the rate of change of distance ρ between the tracking station and the InSight lander. An approximate description of the Doppler signal is given by (Yoder and Standish 1997):

$$\frac{\partial \rho}{\partial t} = \frac{\partial \rho_{EM}}{\partial t} + \frac{\partial \rho_{DSN}}{\partial t} - \frac{\partial}{\partial t}\left[R_z \sin\delta_E + R_s \cos\delta_E \cos(\phi + \lambda - \alpha_E)\right] \tag{5}$$

where ρ_{EM} is the distance from the center of Earth to the center of Mars, ρ_{DSN} is the fraction of distance from the DSN tracking station to the center of Earth parallel to the Earth-Mars direction, R_z is the distance of the lander from the Martian equatorial plane; R_s is the distance from the lander to the Martian spin axis, ϕ is the angle of rotation of Mars about its spin axis, λ is the longitude of the lander, and α_E and δ_E are the right ascension and declination of Earth as viewed from Mars, where declination is the angle from the Martian mean equatorial plane and right ascension is the angle in the Martian equatorial plane measured from where the Sun crosses above the plane (Martian vernal equinox). The Earth-Mars distance is accurately known from radio range measurements to spacecraft in orbit about Mars. The positions of DSN tracking stations are accurately known from Very Long Baseline Interferometry (VLBI) measurements of quasars. The largest signal due to the rotation of Mars comes from the last term in Eq. (5) since ϕ changes 360° per Martian day and has a phase related to the longitude of the lander. Thus two components of the lander position, the longitude and the distance from the spin axis, can be fairly accurately determined from the first tracking pass. The sensitivity to the direction of the Martian spin axis, and hence to precession and nutation, comes from the changes induced on the right ascension and declination of Earth that affect the magnitude and phase of the diurnal signature of the last term of Eq. (5). This signature is reduced when the Earth declination is close to zero (Yseboodt et al. 2017) because the Martian rotation axis is then perpendicular to the Line-of-Sight (LOS). Since the Doppler observable is, to the first order, the projection of the velocity on the LOS, a motion of the spin axis in space at that time results in a negligible contribution in the Doppler signal.

A more detailed Mars rotation model and the list of Mars Orientation Parameters (MOP) are given in Konopliv et al. (2006). The maximum values of the model amplitudes in terms of equivalent displacement on the Martian surface and in the Doppler observable for the InSight science operations period are given in Table 2. The liquid core signatures given in Table 2 are computed assuming an FCN period of 240 days. If the actual FCN period of Mars is closer to a resonant period (for example closer to the ter-annual period of 229 days), the liquid core signature will be larger than the values computed here, while if the FCN period is farther from the resonant periods, the liquid core signature will be smaller. The polar motion signature for InSight is always small (smaller than 0.006 mm/s) because the lander is close to the equator.

Figure 3 shows different quantities related to the geometrical configuration during the InSight mission: the distance between Earth and Mars and the Sun-Earth-Probe (SEP) angle (upper graph) and the declination δ_E of Earth as seen from Mars (lower graph). After the

Table 2 Maximum displacement amplitude on Mars surface, change in the lander position, and signature in the Doppler observable at the InSight location computed for the different Mars orientation parameters (MOP). The models used for the MOP and their numerical values are given in Le Maistre et al. (2012) and in Yseboodt et al. (2017)

MOP	Maximal MOP amplitude on Mars surface	Maximal change in the lander position	Maximal MOP signature in the InSight Doppler data
Nutation in obliquity ($\delta\epsilon$)	10.3 m	10.3 m	0.23 mm/s
Nutation in longitude ($\delta\psi$)	29.4 m	12.3 m	0.38 mm/s
Liquid core amplification (for FCN period of 240 days)	0.7 m on $\delta\psi$, 0.4 m on $\delta\epsilon$	0.4 m	0.01 mm/s
Length-of-day (LOD) variations	11.8 m	11.8 m	0.78 mm/s
Polar motion (PM)	1.2 m	1.2 m	0.006 mm/s

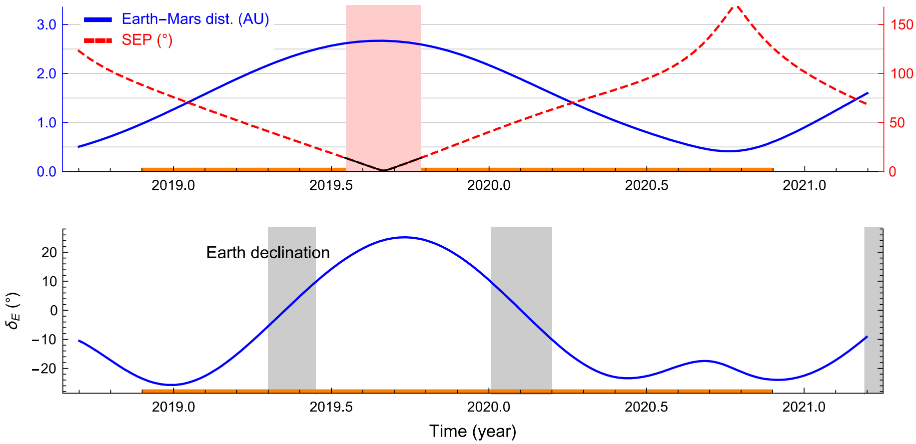

Fig. 3 Distance between the Earth and Mars and declination of Earth as seen from Mars as a function of time, with the times of InSight landed operation indicated in orange. The Sun-Earth-Probe angle is plotted on the first graph in red, the black part of the curve (and the corresponding pink box) being the points where the SEP angle $< 15°$, corresponding to data with a large noise due to the solar plasma. The gray boxes for the Earth declination correspond to time intervals where the Earth declination is smaller than $10°$, which means that the sensitivity to Mars spin axis motion in space is small

landing, the distance between Mars and the Earth increases with a maximum in July-October 2019. A small SEP angle (or elongation angle) $< 15°$, leads to data with large noise due to the solar plasma.

Figure 4 shows the temporal effect of the rigid-body nutations in longitude and obliquity and of the liquid core signature in the Doppler observable. The nutation signature in the Doppler comes from the periodic variations in the nutation amplitude (mostly annual, semi-annual, ter-annual, etc.). In addition, in every signature, there is also a diurnal modulation because the main motion affecting the lander is the diurnal rotation of Mars. The liquid core signature is much smaller than the rigid nutation signature. Its signature in the Doppler observable is more modulated than the other signatures because of the different resonant amplification of the prograde and retrograde nutations. The amplitude and times

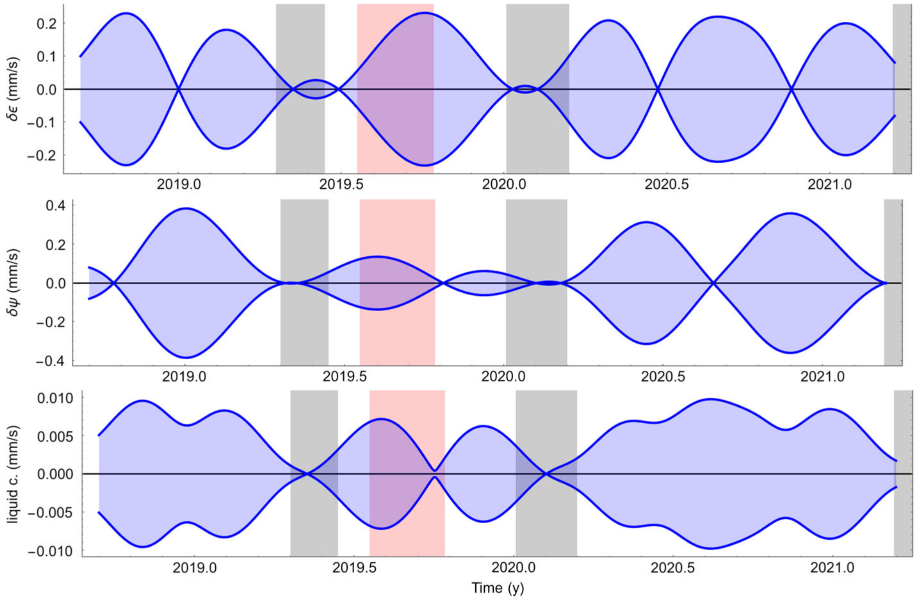

Fig. 4 Temporal evolution of the nutation signature in the Doppler observable (in mm/s) for the InSight lander over the nominal mission duration: the (rigid) nutations in obliquity ($\delta\epsilon$), the (rigid) nutation in longitude ($\delta\psi$) and the liquid core amplification of the nutations (liquid core with a FCN period of 240 days). The gray boxes indicate times when the declination of Earth as seen from Mars is smaller than 10°, when the sensitivity to Mars spin axis motion in space is small. The pink box indicates times when the angular separation of Mars and the Sun as seen from Earth is $< 15°$, when the Doppler measurements are expected to have large noise due to the solar plasma

of the maxima depend on the FCN period (see e.g. Dehant et al. 2000a, 2000b; Van Hoolst et al. 2000a, 2000b).

In addition to changes in the inertial position of the lander due to precession and nutation, the body-fixed position can be affected by solid-body tides. The maximum displacement due to solid tide effects, characterized by Love numbers h_2 and l_2, are 5 mm (Van Hoolst et al. 2003) that is well below the expected uncertainty in estimated body-fixed position.

4 Expected Results

In order to assess the expected results from RISE, an analysis was performed with simulated Doppler data. The simulated data was combined with the available data from Viking lander 1 (covering approximately 1 Martian year from 1976 to 1979) and from Mars Pathfinder (approximately 90 days in 1997). The combined Viking and Pathfinder data serve primarily to extend the data arc for improved estimation of precession.

The lander MGA patterns allow good visibility of Earth for elevation from 5° to 50°. On most days, Earth can be viewed either in the Martian morning on the eastward antenna or in the afternoon on the westward antenna. From simulations over the possible range of view periods, we find that taking data with Earth at low elevation and alternating tracking between eastward and westward antennas when possible provide the best accuracy for estimation of the moment of inertia of the core. The results below used hour-long tracking passes each day alternating between the eastward and westward antenna, using a minimum elevation of

Table 3 Estimated parameters for RISE simulations after one Martian year of operations

Parameter	Symbol	Nominal	Uncertainty
Node longitude at epoch (deg)	ψ_0	81.9683988	0.0000043
Precession rate (mas/year)	$\mathrm{d}\psi/\mathrm{d}t$	−7608.3	1.9
Obliquity at epoch (deg)	ϵ_0	25.1893823	0.0000026
Obliquity rate (mas/year)	$\mathrm{d}\epsilon/\mathrm{d}t$	−2.0	0.26
Liquid-core amplification factor	F	0.07	0.013
FCN rate (degree/day)	ω_{FCN}	−1.50	0.023
Mean spin rate (degree/day)	Ω	350.891985307	0.000000002
Seasonal spin amplitudes (mas)			
	c1	481	6
	s1	−155	4
	c2	−103	5
	s2	−93	4
	c3	−35	4
	s3	−3	3
	c4	−10	2
	s4	−8	2
InSight longitude (degree)	λ	136.165	0.00003
InSight distance to axis (km)	R_s	3388.35	0.00002
InSight distance to equator (km)	R_z	281.19	0.035

10° to account for possible obstructions limiting view of Earth at lower elevation. For each tracking pass Doppler measurements were simulated at 60-second intervals.

The expected measurement noise covariance was calculated depending on the geometry of Earth and Mars for that day, with the correlations between measurements due to solar plasma included. The Doppler noise caused by solar plasma causes the errors of measurements taken at different times to be correlated; the power spectral density of frequency fluctuations from solar plasma follows a Kolmogorov power spectrum with larger fluctuations at longer time scales (Woo et al. 1976). The troposphere noise is uncorrelated for measurements separated by more than 30 seconds (Keihm et al. 2004). Optimal estimation of Martian rotation parameters requires correct treatment of the different type of noise.

Table 3 lists the parameters estimated, their nominal values (from Konopliv et al. 2016), and estimated uncertainty after the end of the one Martian year of InSight data acquisition.

Assuming that the FCN period is −240 days, it is expected that the FCN rate will be known with an uncertainty of 0.023 deg/day, which corresponds to a ∼5 days uncertainty on the FCN period, from which the core radius can be estimated with an uncertainty of about 100 km (see Fig. 1a) if the mantle compositions and temperature end-members introduced in Sect. 2 are assumed. However this uncertainty in core radius depends on the assumption of core being hydrostatic. Taking uncertainty of the core shape into account leads to a larger uncertainty in the core radius. The uncertainty in core radius inferred from the expected accuracy in the amplification factor F is 150 km (Fig. 1b). This uncertainty is much less sensitive to the composition and temperature of the mantle than the FCN period. The uncertainty in the FCN period ($\tau_{FCN} = \Omega/\omega_{FCN}$) is very dependent on the actual value of Mars FCN period (the closer to the ter-annual forcing period the more accurately τ_{FCN} will be determined) and could therefore be larger (or smaller) than predicted here. Nevertheless, an uncertainty smaller than 1 day, which is required to obtain meaningful inferences about the mantle quantities (see Fig. 1a), seems unlikely to be achieved unless the FCN is very close to the ter-annual period.

RISE will determine the precession rate with accuracy less than 2 mas/yr or 0.025% of its nominal value (see Table 3). This is only slightly better than the current 2.1 mas/yr uncertainty (Konopliv et al. 2016) and will therefore not provide much new information. RISE will reduce the uncertainty in the amplitudes of the seasonal spin variations by about 50% with respect to the latest solutions (Konopliv et al. 2016), which will help constrain the mass budget between the atmosphere and icecaps (Spiga et al. 2018, this issue).

5 Cartographic Location

The estimated location of InSight after landing will yield a superb tie between the cartographic coordinates from imaging and the inertial reference frame in which the positions of orbiting spacecraft are determined. This is critically important for landing and operating spacecraft on Mars and for defining surface coordinate systems. Previous landers have provided ties between their locations determined from radio tracking data with respect to surface features using either images from orbiting spacecraft; from images taken while landing; or from images from cameras on the landers (e.g., Golombek et al. 1997, 1999a, 1999b; Arvidson et al. 2004a, 2004b). Since the Mars Orbiter Laser Altimeter (MOLA) updated the Mars cartographic frame (positive east planetocentric coordinate system referenced to the IAU/IAG 2000 frame, which is compatible with the inertial coordinates used by spacecraft navigation teams, Smith et al. 2001), localization after landing by the Mars Exploration Rovers (MER) has shown that the tie consistency between the two frames is roughly 100–300 m (Arvidson et al. 2004a, 2004b).

In the past, the largest uncertainty in the relation of cartographic positions and inertial coordinates has been in the uncertainty of the reference longitude and the rotation angle (from Eq. (5)) at a reference time, designated ϕ_0, where the reference time is 01-January-2000 @ 12:00. With the longitude origin defined by the center of the crater Airy-0, the accuracy of ϕ_0 has been limited by the resolution of camera images of the crater and by uncertainty in the pointing direction of the cameras with respect to inertial space. This has resulted in uncertainty in ϕ_0 corresponding to uncertainty in surface feature position of $\sim$100 m. In contrast, the longitudes of Mars landers determined by radio Doppler measurements have internal consistency better than 10 m. Because the Viking 1 lander position has been determined both with radio Doppler and imaging, recently the IAU Working Group on Cartographic Coordinates and Rotational Elements has adopted use of the longitude of the Viking 1 lander as defining, with a value as consistent with the longitude of center of Airy-0 being zero as currently possible (Kuchynka et al. 2014; Archinal et al. 2018).

By the end of the InSight mission, the cumulative Doppler measurements for RISE will determine the InSight position very accurately (see Table 3). The uncertainty in the distance from the spin axis, R_s, will be 2 cm, about 5 times better than for any previous lander. The uncertainty in longitude will be about 0.00003°, corresponding to about 2 m in displacement, limited mainly by uncertainty in the Martian rotation rate times the 40 years from the time of the Viking lander to the InSight landing date. If InSight is chosen to become a new reference for longitude, then future landers will be able to have longitude determined to 2 cm accuracy. The distance from the equatorial plane, R_z, will be known to 35 m accuracy from the Doppler data only, and could be reduced to about one meter (or 0.00002° in latitude) from the combination of the Doppler data and topography (Le Maistre 2016).

The location of the lander with respect to cartographic features will be determined by imaging the spacecraft on the surface with the High-Resolution Imaging Science Experiment (HiRISE) camera on the Mars Reconnaissance Orbiter and/or by identifying common features that can be seen in both surface and orbital images. The positions for Mars Pathfinder, Phoenix, and the Mars Exploration Rovers were determined comparing images from the lander with images from orbiters (e.g. Golombek et al. 1997, 1999a, 1999b; Arvidson et al. 2004a, 2004b). Phoenix and Curiosity were both imaged directly by HiRISE after landing, as have all landers (e.g., Parker et al. 2012, 2013).

In order to aid in imaging of InSight by HiRISE, the location will be determined from the first two sols of Doppler tracking data. Thirty minutes of Doppler data will be acquired on the first sol after landing, followed by thirty minutes on the second sol. These data are sufficient to determine the lander longitude and distance from the spin axis, R_s, with accuracy of about 20 m (or about 0.0004° in longitude). The distance from the equator, R_z, and hence the latitude, is not well determined from Doppler data given that the rate of change of distance (Eq. (5)) is predominantly due to the Martian diurnal rotation and is not dependent on R_z. Instead R_z will be determined by combining the Doppler data with topographical models (Le Maistre 2016). The lander coordinates in the equatorial plane, λ and R_s, estimated from the Doppler data, will be used together with their uncertainties to determine the range of possible R_z values such that the lander is on the surface of the planet, as defined by the topography. By combining the first two sols of Doppler data with knowledge of the topography from the gridded MOLA elevations (Smith et al. 2001), R_z will be determined with 250 m accuracy. This will determine the latitude with accuracy 0.004°. A better estimation of R_z could be obtained from digital elevation models of higher precision and spatial resolution such as those derived from Mars Express High Resolution Stereo Camera (HRSC) (Gwinner et al. 2010) and the MRO Context Camera (CTX) (Fergason et al. 2017), that have been produced for the InSight landing site (Golombek et al. 2017).

HiRISE images are 5 km wide, so this initial location should be accurate enough to image the lander on the first try. Once a HiRISE image is acquired, the image can be georeferenced onto landing site maps, that have been georeferenced in a pyramid starting with MOLA elevation maps, 463 m/pixel; HRSC, 12.5 m/pixel; CTX 5–6 m/pixel; and HiRISE ~0.25–0.3 m/pixel images (Golombek et al. 2017) to determine the cartographic location of the lander. This will also help provide context for the geology and physical properties investigations (Golombek et al. 2018).

6 RISE Follow-on: The LaRa Experiment

Two years after InSight landing, at the end of its nominal mission, the ESA-ROSCOSMOS ExoMars 2020 mission will land on the other side of Mars at a higher latitude (18.20° north latitude, 335.45° east longitude). The ExoMars surface platform will carry 13 scientific instruments including the Belgian Lander Radio-science (LaRa) instrument. Like RISE, LaRa will take Doppler measurements using an X-band radio transponder to improve our knowledge about Mars' rotation and interior structure (Dehant et al. 2009, 2011; Le Maistre et al. 2012). The combination of RISE and LaRa data will allow for an even more accurate estimation of the effect of the liquid core on the nutation than from each experiment alone and will further improve our knowledge about the interior structure of Mars. Moreover, because of its higher latitude, LaRa could help to complete the rotation model of Mars by measuring for the first time[1] the polar motion of Mars. The benefits of a combination of RISE and LaRa will be investigated in a future work.

7 Conclusion

The RISE experiment is specifically designed to measure for the first time the effect of the liquid core on the nutation of Mars. Accurate knowledge of nutation will reveal more information about the interior structure of Mars and in particular about the core radius and moment of inertia than is currently known (e.g. Dehant et al. 2000a, 2000b). More precise constraints on the core radius and density can be obtained if data from RISE are combined with data from the seismometer (SEIS) and heat flow probe instruments (HP^3), since both experiments are expected to constrain the composition and thermal state of Mars' silicate shell. RISE will also improve the global rotation model of Mars, from which a more precise moment of inertia of the planet can be determined and knowledge about the global atmosphere dynamics be inferred. Finally, RISE will provide a superb tie between the cartographic and inertial reference frames of Mars.

Acknowledgements This research was carried out in part by the InSight Project at the Jet Propulsion Laboratory, California Institute of Technology, under contract with the National Aeronautics and Space Administration; and in part at the Royal Observatory of Belgium with financial support by the Belgian PRODEX program managed by the European Space Agency in collaboration with the Belgian Federal Science Policy Office. This is InSight Contribution Number 53.

References

B.A. Archinal, C.H. Acton, M.F. A'Hearn, A. Conrad et al., Report of the IAU working group on cartographic coordinates and rotational elements: 2015. Celest. Mech. Dyn. Astron. **130**(3), 22 (2018). https://doi.org/10.1007/s10569-017-9805-5

R.E. Arvidson, R.C. Anderson, P. Bartlett, J.F. Bell et al., Localization and physical properties experiments conducted by Spirit at Gusev crater. Science **305**, 821–824 (2004a)

R.E. Arvidson, R.C. Anderson, P. Bartlett, J.F. Bell et al., Localization and physical properties experiments conducted by opportunity at Meridiani Planum. Science **306**, 1730–1733 (2004b)

S.W. Asmar, J.W. Armstrong, L. Iess, P. Tortora, Spacecraft Doppler tracking: Noise budget and accuracy achievable in precision radio science observations. Radio Sci. **40**, RS2001 (2005). https://doi.org/10.1029/2004RS003101

W.B. Banerdt et al., The InSight mission. Space Sci. Rev. (2018), this issue

Y.E. Bar-Sever, C.S. Jacobs, S. Keihm, G.E. Lanyi et al., Atmospheric media calibration for the deep space network. Proc. IEEE **95**, 2180–2192 (2007)

J.-P. Barriot, V. Dehant, J.-C. Cerisier, W. Folkner et al., NEIGE: NetLander ionosphere and geodesy experiment. Adv. Space Res. **28**, 1237–1249 (2001). https://doi.org/10.1016/S0273-1177(01)00295-2

N. Bergeot, O. Witasse, W. Kofman, C. Grima et al., Study of the total electron content in Mars ionosphere from MARSIS data set, in *EGU General Assembly 2016*, Vienna, Austria (2016)

A. Cazenave, G. Balmino, Meteorological effects on the seasonal variations on the rotation of Mars. Geophys. Res. Lett. **8**, 245–248 (1981)

B.F. Chao, D.P. Rubincam, Variations of Mars' gravitational field and rotation due to seasonal CO2 exchange. J. Geophys. Res. **95**(B9), 14755–14760 (1990)

S. Chapman, The absorption and dissociative or ionizing effect of monochromatic radiation in an atmosphere on a rotating Earth. Proc. Phys. Soc. **43**, 26–45 (1931)

J.A.D. Connolly, Computation of phase equilibria by linear programming: A tool for geodynamic modeling and its application to subduction zone decarbonation. Earth Planet. Sci. Lett. **236**, 524–541 (2005). https://doi.org/10.1016/j.epsl.2005.04.033

[1] A first low accuracy estimate of polar motion amplitudes has been inferred from gravity degree-2 coefficients by Konopliv et al. (2006), but no direct measurements of it has been performed until now.

F.A. Dahlen, J. Tromp, *Theoretical Global Seismology* (Princeton University Press, Princeton, 1998)
P. Defraigne, O. de Viron, V. Dehant, T. Van Hoolst, F. Hourdin, Mars rotation variations induced by atmospheric CO2 and winds. J. Geophys. Res., Planets **105**, 24563–24570 (2000). https://doi.org/10.1029/1999JE001227
P. Defraigne, A. Rivoldini, T. Van Hoolst, V. Dehant, Mars nutation resonance due to free inner core nutation. J. Geophys. Res., Planets **108**(E12), 5128 (2003). https://doi.org/10.1029/2003JE002145
V. Dehant, P.M. Mathews, *Precession, Nutation and Wobble of the Earth* (Cambridge University Press, Cambridge, 2015)
V. Dehant, P. Defraigne, T. Van Hoolst, Computation of Mars' transfer function for nutation tides and surface loading. Phys. Earth Planet. Inter. **117**, 385–395 (2000a). https://doi.org/10.1016/S0031-9201(99)00108-9
V. Dehant, T. Van Hoolst, P. Defraigne, Comparison between the nutations of the planet Mars and the nutations of the Earth. Geophys. Surv. **21**, 89–110 (2000b)
V. Dehant, W. Folkner, E. Renotte, D. Orban et al., Lander radioscience for obtaining the rotation and orientation of Mars. Planet. Space Sci. **57**, 1050–1067 (2009). https://doi.org/10.1016/j.pss.2008.08.009
V. Dehant, S. Le Maistre, A. Rivoldini, M. Yseboodt et al., Revealing Mars' deep interior: Future geodesy missions using radio links between landers, orbiters, and the Earth. Planet. Space Sci. **57**, 1069–1081 (2011). https://doi.org/10.1016/j.pss.2010.03.014
G. Dreibus, H. Wanke, Mars, a volatile-rich planet. Meteoritics **20**, 367–381 (1985)
R. Fergason, R.L. Kirk, G. Cushing, D.M. Galuzska et al., Analysis of local slopes at the InSight landing site on Mars. Space Sci. Rev. **211**, 109–133 (2017). https://doi.org/10.1007/s11214-016-0292-x
W.M. Folkner, C.F. Yoder, D.N. Yuan, E.M. Standish, R.A. Preston, Interior structure and seasonal mass redistribution of Mars from radio tracking of Mars Pathfinder. Science **278**, 1749–1752 (1997)
A. Genova, S. Goossens, F.G. Lemoine, E. Mazarico et al., Seasonal and static gravity field of Mars from MGS, Mars Odyssey and MRO radio science. Icarus **272**, 228–245 (2016). https://doi.org/10.1016/j.icarus.2016.02.050
M.P. Golombek, R.A. Cook, T. Economou, W. Folkner et al., Overview of the Mars Pathfinder mission and assessment of landing site predictions. Science **278**, 1743–1748 (1997)
M.P. Golombek, R.C. Anderson, J.R. Barnes, J.F. Bell et al., Overview of the Mars Pathfinder mission: Launch through landing, surface operations, data sets, and science results. J. Geophys. Res. **104**, 8523–8553 (1999a)
M.P. Golombek, H.J. Moore, A.F.C. Haldemann, T.J. Parker, J.T. Schofield, Assessment of Mars Pathfinder landing site predictions. J. Geophys. Res. **104**, 8585–8594 (1999b)
M.P. Golombek, D. Kipp, N. Warner, I.J. Daubar et al., Selection of the InSight landing site. Space Sci. Rev. **211**, 5–95 (2017). https://doi.org/10.1007/s11214-016-0321-9
M.P. Golombek, M. Grott, G. Kargl, J. Andrade et al., Geology and physical properties investigations by the InSight lander. Space Sci. Rev. (2018), this issue. https://doi.org/10.1007/s11214-018-0512-7
K. Gwinner, F. Scholten, F. Preusker, S. Elgner et al., Topography of Mars from global mapping by HRSC high-resolution digital terrain models and orthoimages: Characteristics and performance. Earth Planet. Sci. Lett. **294**, 506–519 (2010). https://doi.org/10.1016/j.epsl.2009.11.007
Ö. Karatekin, T. Van Hoolst, J. Tastet, O. de Viron, V. Dehant, The effects of seasonal mass redistribution and interior structure on length-of-day variations of Mars. Adv. Space Res. **38**, 739–744 (2006). https://doi.org/10.1016/j.asr.2005.03.117
Ö. Karatekin, O. de Viron, S. Lambert, P. Rosenblatt et al., Atmospheric angular momentum variations of Earth, Mars and Venus at seasonal time scales. Planet. Space Sci. **59**, 923–933 (2011). https://doi.org/10.1016/j.pss.2010.09.010
S.J. Keihm, A. Tanner, H. Rosenberger, Measurements and calibration of tropospheric delay at Goldstone from the Cassini media calibration system, in *Interplanetary Network Progress Report 42-158* (2004)
A. Khan, C. Liebske, A. Rozel, A. Rivoldini et al., A geophysical perspective on the bulk composition of Mars. J. Geophys. Res. **123**(2), 575–611 (2018). https://doi.org/10.1002/2017JE005371
A.S. Konopliv, C.F. Yoder, E.M. Standish, D.N. Yuan, W.L. Sjogren, A global solution for the Mars static and seasonal gravity, Mars orientation, Phobos and Deimos masses, and Mars ephemeris. Icarus **182**, 23–50 (2006)
A.S. Konopliv, S.W. Asmar, W.M. Folkner, Ö. Karatekin et al., Mars high resolution gravity fields from MRO, Mars seasonal gravity, and other dynamical parameters. Icarus **211**, 401–428 (2011)
A.S. Konopliv, R.S. Park, W.M. Folkner, An improved JPL Mars gravity field and orientation from Mars orbiter and lander tracking data. Icarus **274**, 253–260 (2016). https://doi.org/10.1016/j.icarus.2016.02.052
P. Kuchynka, W.M. Folkner, A.S. Konopliv, R.S. Park, S. Le Maistre, V. Dehant, New constraints on Mars rotation determined from radiometric tracking of the opportunity Mars exploration rover. Icarus **229**, 340–347 (2014). https://doi.org/10.1016/j.icarus.2013.11.015

S. Le Maistre, InSight coordinates determination from direct-to-Earth radio-tracking and Mars topography model. Planet. Space Sci. **121**, 1–9 (2016). https://doi.org/10.1016/j.pss.2015.11.003

S. Le Maistre, P. Rosenblatt, A. Rivoldini, V. Dehant et al., Lander radio science experiment with a direct link between Mars and the Earth. Planet. Space Sci. **68**, 105–122 (2012). https://doi.org/10.1016/j.pss.2011.12.020

R.J. Lillis, D.A. Brain, S.L. England, P. Withers et al., Total electron content in the Mars ionosphere: Temporal studies and dependence on solar EUV flux. J. Geophys. Res. Space Phys. **115**, A11314 (2010). https://doi.org/10.1029/2010JA015698

K. Lodders, B. Fegley, An oxygen isotope model for the composition of Mars. Icarus **126**, 373–394 (1997). https://doi.org/10.1006/icar.1996.5653

P. Lognonne, W.B. Banerdt, D. Giardini, W.T. Pike et al., SEIS: The seismic experiment for internal structure on InSight. Space Sci. Rev. (2018), this issue

A.J. Mannucci, B.D. Wilson, D.N. Yuan, C.H. Ho et al., A global mapping technique for GPS-derived ionospheric total electron content. Radio Sci. **33**, 565–582 (1998)

P.M. Mathews, B.A. Buffett, T.A. Herring, I.I. Shapiro, Forced nutations of the Earth: Influence of inner core dynamics: 1. Theory. J. Geophys. Res., Solid Earth **96**(B5), 8219–8242 (1991a)

P.M. Mathews, B.A. Buffett, T.A. Herring, I.I. Shapiro, Forced nutations of the Earth: Influence of inner core dynamics, 2. Numerical results and comparisons. J. Geophys. Res., Solid Earth **96**(B5), 8243–8257 (1991b). https://doi.org/10.1029/90JB01956

R.K. Mohapatra, S.V.S. Murty, Precursors of Mars: Constraints from nitrogen and oxygen isotopic compositions of Martian meteorites. Meteorit. Planet. Sci. **38**(2), 225–241 (2003). https://doi.org/10.1111/j.1945-5100.2003.tb00261.x

J.W. Morgan, E. Anders, Chemical composition of Mars. Geochim. Cosmochim. Acta **43**(10), 1601–1610 (1979). https://doi.org/10.1016/0016-7037(79)90180-7

P. Morgan, S.E. Smrekar, R. Lorenz, M. Grott, O. Kroemer, O. Müller, Potential effects of surface temperature variations and disturbances and thermal convection on the Mars InSight HP^3 heat-flow determination. Space Sci. Rev. **211**, 277 (2017). https://doi.org/10.1007/s11214-017-0388-y

M.P. Panning, P. Lognonne, W.B. Banerdt, R. Garcia et al., Planned products of the Mars structure service for the InSight mission to Mars. Space Sci. Rev. **211**, 611–650 (2017). https://doi.org/10.1007/s11214-016-0317-5

T.J. Parker, F.J. Calef, M.P. Golombek, T.M. Hare, High-resolution basemaps for localization, mission planning, and geologic mapping at Meridiani Planum and Gale crater, in *The 43rd Lunar and Planetary Science Conference* (Lunar and Planetary Institute, Houston, 2012). Abstract #2535

T.J. Parker, M.C. Malin, F.J. Calef, R.G. Deen et al., Localization and 'contextualization' of Curiosity in Gale crater, and other landed Mars missions, in *The 44th Lunar and Planetary Science Conference* (Lunar and Planetary Institute, Houston, 2013). Abstract #2534

A.C. Plesa, M. Grott, N. Tosi, D. Breuer et al., How large are present-day heat flux variations across the surface of Mars? J. Geophys. Res., Planets **121**, 2386–2403 (2016). https://doi.org/10.1002/2016JE005126

A. Rivoldini, T. Van Hoolst, The interior structure of Mercury constrained by the low-degree gravity field and the rotation of Mercury. Earth Planet. Sci. Lett. **377**, 62–72 (2013). https://doi.org/10.1016/j.epsl.2013.07.021

A. Rivoldini, T. Van Hoolst, O. Verhoeven, A. Mocquet, V. Dehant, Geodesy constraints on the interior structure and composition of Mars. Icarus **213**, 451–472 (2011). https://doi.org/10.1016/j.icarus.2011.03.024

F. Roosbeek, Analytical developments of rigid Mars nutation and tide generating potential series. Celest. Mech. Dyn. Astron. **75**, 287–300 (1999)

C. Sanloup, A. Jambon, P. Gillet, A simple chondritic model of Mars. Phys. Earth Planet. Inter. **112**, 43–54 (1999). https://doi.org/10.1016/S0031-9201(98)00175-7

T. Sasao, S. Okubo, M. Saito, A simple theory on the dynamical effects of a stratified fluid core upon nutational motion of the Earth, in *Symposium-International Astronomical Union*, vol. 78 (Cambridge University Press, Cambridge, 1980), pp. 165–183

D.E. Smith, M.T. Zuber, H.V. Frey, J.B. Garvin et al., Mars Orbiter Laser Altimeter (MOLA): Experiment summary after the first year of global mapping of Mars. J. Geophys. Res. **106**, 23689–23722 (2001)

A. Spiga, N. Teanby, A. Lucas, B. Kenda et al., Atmospheric science with InSight. Space Sci. Rev. (2018), this issue

T. Spohn, M. Grott et al., The heat flow and physical properties package (HP^3) for the InSight mission. Space Sci. Rev. (2018), this issue. https://doi.org/10.1007/s11214-018-0531-4

G.J. Taylor, The bulk composition of Mars. Chem. Erde **73**, 401–420 (2013). https://doi.org/10.1016/j.chemer.2013.09.006

E. Van den Acker, T. Van Hoolst, O. de Viron, P. Defraigne et al., Influence of the winds and of the CO2 mass exchange between the atmosphere and the polar ice caps on Mars' rotation. J. Geophys. Res. **107**(E7), 5055 (2002). https://doi.org/10.1029/2000JE001539

T. Van Hoolst, V. Dehant, Influence of triaxiality and second-order terms in flattenings on the rotation of terrestrial planets: I. Formalism and rotational normal modes. Phys. Earth Planet. Inter. **134**, 17–33 (2002)

T. Van Hoolst, V. Dehant, P. Defraigne, Sensitivity of the free core nutation and the Chandler Wobble to changes in the interior structure of Mars. Phys. Earth Planet. Inter. **117**, 397–405 (2000a)

T. Van Hoolst, V. Dehant, P. Defraigne, Chandler Wobble and free core nutation for Mars. Planet. Space Sci. **48**, 1145–1151 (2000b)

T. Van Hoolst, V. Dehant, F. Roosbeek, P. Lognonné, Tidally induced surface displacements, external potential variations, and gravity variations on Mars. Icarus **161**, 281–296 (2003). https://doi.org/10.1016/S0019-1035(02)00045-3

M.A. Wieczorek, M.T. Zuber, Thickness of the Martian crust: Improved constraints from geoid-to-topography ratios. J. Geophys. Res. **109**, E1 (2014). https://doi.org/10.1029/2003JE002153

R. Woo, F.-C. Yang, K.W. Yip, W.B. Kendall, Measurements of large-scale density fluctuations in the solar wind using dual-frequency phase scintillations. Astrophys. J. **210**, 568–574 (1976)

C.F. Yoder, E.M. Standish, Martian precession and rotation from Viking lander range data. J. Geophys. Res. **102**(E2), 4065–4080 (1997)

C.F. Yoder, A.S. Konopliv, D.N. Yuan, E.M. Standish, W.M. Folkner, Fluid core size of Mars from detection of the solar tide. Science **300**, 299–303 (2003). https://doi.org/10.1126/science.1079645

M. Yseboodt, V. Dehant, M.J. Péters, Signatures of the Martian rotation parameters in the Doppler and range observables. Planet. Space Sci. **144**, 74–88 (2017)